Dalton Transactions

Accepted Manuscript

ROYAL SOCIETY OF CHEMISTRY

www.rsc.org/dalton

Dalton Transactions

ARTICLE

The Electronic Structures and Photophysical Properties of Platinum Complexes with CˆNˆN Ligands: Influence of Carborane Substituent

Received 00th January 20xx,
Accepted 00th January 20xx

DOI: 10.1039/x0xx00000x

www.rsc.org/

Wenting Zhang[a], Yafei Luo[a], Yanyan Xu[a], Li Tian[a], Ming Li[a], Rongxing He[a] and Wei Shen[a*]

Carboranes has attracted increasing interest in the scientific community due to their remarkable structures and strong electron-withdrawing abilities. In this article, four platinum complexes: [(CˆNˆN)PtC≡CPh](**1**), [(CˆNˆN)PtC≡C-TPA](**2**), [(CˆNˆN)PtC≡C-TAB](**3**), [(CˆNˆN)PtC≡C-CB](**4**), (where TPA= triphenylamine, TAB= triarylboryl, CB= *o*-carborane), have been calculated via the density functional theory (DFT) and the time-dependent density functional theory (TDDFT) methods to mainly explore the influence of carborane subtituents on electron strctures, photophysics properties and radiative decay processes. The calculated results reveal that **2** with electron-donating triphenylamine has a low radiative decay rate constant and a red-shifted emission band, but **3** and **4** containing electron-withdrawing triarylboryl and *o*-carborane exhibit the opposite properties, especially **4** , supposed to have the highest phosphorescence quantum yield with the smallest nonradiative decay rate constant. These findings successfully illustrated the structure–property relationship and the designed complexe **4** with carborane can server as the highly efficient phosphorescent material in the future.

Introduction

There is increased interest in the development of organic light-emitting diodes (OLEDs) doped with phosphorescent transition metal compounds, which can achieve a theoretical internal quantum efficiency of almost 100% owing to the full mixing of singlet and triplet excitons caused by strong spin–orbit coupling from the heavy metal atoms.[1-5] Among the transition metal complexes reported, cyclometalated platinum(II) complexes have been extensively investigated. As well known, a variety of charge-transfer (CT) excited states, including ILCT (intraligand charge transfer), LLCT (ligand-to-ligand charge transfer), and MLCT (metal-to-ligand charge transfer), have been reported in platinum(II) complexes.[6-9] In addition, due to the dsp^2 hybridization, these platinum(II) complexes usually have a tendency to form the square-planar structure and then discourages D2d distortion, which is likely to facilitate electron delocalization and result in radiationless decay,[10, 11] Moreover, as reported, t the photophysical properties of the transition metal complexes can be effectively tuned by structurally modifying the coordinated ligands. [3, 12, 13] Owing to these properties, the platinum(II) complexes have been generally recognized as potential phosphors applied in electroluminescent devices with high phosphorescence quantum efficiencies.

Among the cyclometalated square-planar platinum(II) complexes, tridentate cyclometalated platinum(II) acetylide complexes have been extensively explored due to their rich spectroscopic properties.[14, 15] Compared to the corresponding platinum terpyridyl complexes, these complexes possess relatively intense emission partially due to weakened radiationless decay, which can be ascribed to the less-distorted square-planar geometry.[16, 17] In these series, acetylide moieties, as rigid π-conjugated bridging components, help to increase the emission quantum yield because of the strong-field nature and open a way to new systems containing a variety of host receptors.[18] For improving electroluminescent efficiency, one feasible method is to introduce different substituents into the auxiliary ligands to increase the rigidity of molecules. A series of 6-aryl-2,2'-bypyridine tridentate cyclometalated platinum(II) acetylide complexes have been synthesized by Che and co-workers[19], as reported, the excited state properties and luminescence properties such as phosphorescence quantum efficiency, color purity could be optimized correspondingly by means of variation of the substituent in the σ-alkynyl auxiliary.[20]

As a strong electron-withdrawing group with the three-dimensional icosahedral cage structure, carborane has already been widely applied in the fields of biological

[a]*College of Chemistry and Chemical Engineering, Southwest University, Chongqing 400715 (P.R. China)*
E-mail addresses: shenw@swu.edu.cn (W Shen)
Electronic Supplementary Information (ESI) available: [details of any supplementary information available should be included here]. See DOI: 10.1039/x0xx00000x

sciences, medical imaging, materials science and medicinal chemistry.[21] Actually, it is common to incorporate strong electron-withdrawing groups, such as triarylboryl, into Ir(Ⅲ) and Pt(II) complexes to modulate emission color and increase the phosphorescent efficiency.[22-25] Nowadays, there has already been some researches about carboranes in organic light emitting diodes (OLEDs).[26, 27] However, further theoretical studies on carboranes in OLED field are scarce and most are limited to the utilization of ortho-carborane (*o*-carborane). In recent researches, some transition metal complexes are reported to exhibit lower phosphorescence quantum yield in solid state or in high concentration solution due to the intermolecular interactions between phosphorescent emitter molecules and thereby leading to a triplet-triplet annihilation and concentration quenching.[28] The bulkiness of carborane can hinder the intermolecular interactions, restraining triplet−triplet annihilation.[29, 30]

In our work, we have conducted a theoretical study on four CˆNˆN platinum complexes: [(CˆNˆN)PtC≡CPh](**1**), [(CˆNˆN)PtC≡C-TPA](**2**), [(CˆNˆN)PtC≡C-TAB](**3**), [(CˆNˆN)PtC≡C-CB](**4**), (where TPA= triphenylamine, TAB= triarylboryl, CB= *o*-carborane) and the chemical structures have been presented in Scheme 1. Thereinto, the complex **1** was already synthesized and characterized by Che and co-workers,[19] then based on complex **1** without benzene auxiliary substituent, we added *o*-carborane into the acetylide moiety to design complex **4**. Additionally, to further explore the influence of carborane, we introduce triphenylamine and triarylboryl, the typical electron-donating and electron-withdrawing groups, to design complexes **2** and **3**. We expect that the strategy reported herein could provide valuable information for designing original and highly-efficient OLED materials in the future.

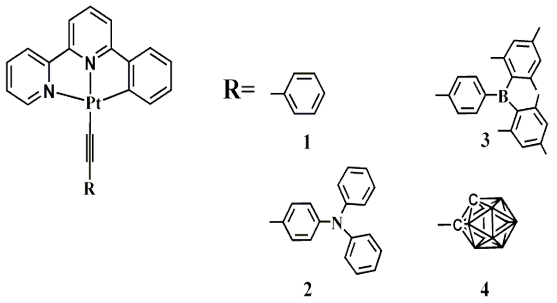

Scheme 1 Chemical Structures of **1**−**4**

Computational details

Geometry optimizations were performed on the ground states and triplet excited states of **1-4** by using the density functional theory (DFT)[31, 32]. In this work, to find a suitable functional level for our investigated systems, three different functional levels (M062X[33], PBE0[34] and B3LYP[35]) were carried out to optimize the ground state of complex **1** in dichloromethane (CH_2Cl_2), as a result, PBE0 with 6-31G* basis set[36] is more accurate in reproducing the experimental data than the other two functionals (Table S1). Based on the optimized geometries, the time-dependent density functional theory (TDDFT) method[37-39] associated with the polarizable continuun model (PCM)[40] in CH_2Cl_2 was employed to investigate the absorption and emission properties. In the TDDFT calculations, the PBE0 was the most suitable functional (Table S2). Meanwhile, the 6-31G* basis set was used for all the light atoms and the LANL2DZ basis set[41] was adopted for the Pt atom. All the above calculations were performed with the Gaussian 09 software package.[42]

In general, the phosphorescence quantum yield (Φ_{pL}) is mainly governed by two factors, including radiative rate (k_r) and non-radiative rate (k_{nr}) constants, which can be defined as eq (1):

$$\Phi_{pL} = \frac{k_r}{k_r + k_{nr}} \qquad (1)$$

Thus lager k_r and smaller k_{nr} are desirable for obtaining a higher Φ_{pL}.

Based on the energy gap law, the nonradiative decay rate constant k_{nr} can be expressed as below

$$k_{nr}(T_m \rightarrow S_0) \propto \exp\{-\beta[E(T_m) - E(S_0)]\} \qquad (2)$$

where the parameter β is related to the structural distortion between the involved potential energy surfaces (PESs) of the ground and the excited triplet states. Hence, it is considered that larger structural distortions cause larger k_{nr}. In addition, as the energy gap between T_m and S_0 states decreases, the nonradiative decay rate decreases.

On the other hand, the radiative decay rate constant κ_r^i and radiative decay lifetimes τ_r^i from triplet substates i ($i = 1,2,3$) of the lowest triplet emissive state to the ground state can be calculated on the basis of perturbation theory as:

$$\kappa_r^i = \frac{1}{\tau_r^i} = \kappa_r(S_0, T_1^i) = \frac{4{\alpha_0}^3}{3t_0}\Delta E_{S_0-T_1^i}{}^3 \sum_{j\in\{x,y,z\}} \left|M_j^i\right|^2 \qquad (3)$$

Where $\Delta E_{S_0-T_1^i}$ is the energy of $T_1^i \rightarrow S_0$ transition, α_0 is the fine-structure constant, $t_0 = (4\pi\varepsilon_0)^2\hbar^3/m_e e^4$ and M_j^i is the transition dipole moment with spin-orbit coupling (SOC), which can be expressed as eq (4)

$$M_j^i = \sum_{n=0}^{\infty} \frac{\langle S_0|\hat{\mu}_j|S_n\rangle\langle S_n|\hat{H}_{SO}|T_1^i\rangle}{E(S_n) - E(T_1)} + \sum_{m=1}^{\infty} \frac{\langle S_0|\hat{H}_{SO}|T_m\rangle\langle T_m|\hat{\mu}_j|T_1^i\rangle}{E(T_m) - E(S_0)} \qquad (4)$$

Where $\hat{H}_{SO}$ is the spin-orbital Hamiltonian and $\hat{\mu}_j$ refers to the transition electric dipole moment. The two parts are

separate between the spin manifolds and the relative importance of each term can be qualitatively deduced through eq (4) .It is found that the energy differences between S_0 and T_m are much greater than the energy differences between S_n and T_1 and the transition dipole moments between S_0 and S_n are much greater than transition dipole moments between T_m and T_1. Thereby, the former is much larger in eq (4) and regarded as the main factor controlling the M_j^i value.

Assuming a thermal population distribution governed by Boltzmann statistics of the triplet sublevels, the overall observable rate is given by the following equation:

$$\kappa^r = \frac{\kappa_1^r + \kappa_2^r exp\left(-\mathrm{ZFS}_{1,2}/\kappa_B T\right) + \kappa_3^r exp\left(-\mathrm{ZFS}_{1,3}/\kappa_B T\right)}{1 + exp\left(-\mathrm{ZFS}_{1,2}/\kappa_B T\right) + exp\left(-\mathrm{ZFS}_{1,3}/\kappa_B T\right)} \quad (5)$$

where ZFS is the zero-field splitting between each of the three sublevels (1, 2, 3). The $ZFS_{1,3}$ for phosphorescent emitters is typically <200 cm^{-1}.[43] If $k_BT \gg ZFS_{1,3}$, then the previous equation can be reduced to

$$\kappa^r = \frac{1}{3}\sum_{i=1}^{3}\kappa_i^r \quad (6)$$

To evaluate eq (3), we have calculated the M_j^i transition moment by the TDDFT method. The calculations are performed on optimized T1 geometries in the Amsterdam Density Functional package (ADF 2014.04),[44, 45] using the TDDFT/PBE0 including SOC calculations with zero order regular approximation (ZORA) Hamiltonian on the basis of perturbation theory.[46] Since full SOC-TDDFT is theoretically a more accurate approach, it is more computationally demanding than a perturbation based on the scalar relativistic orbitals for the same number of excitations. An all-electron triple-zeta + polarization (TZP) basis set was used for Pt, while the double-zeta + polarization (DZP) was used for all other atoms. No core electrons were frozen during the SCF calculation and a Becke grid of "good" quality was used for the numerical integration. Moreover, all the calculations are conducted with Conductor like screening model (COSMO)[47, 48] of solvation with CH_2Cl_2 parameters taken in account.

Results and discussion

Geometries of S_0 and T_1 States

The optimized structure of complex **1** in the ground state (S_0) is depicted in Figure 1. As well known, the differences observed in the photophysical properties of these complexes mainly depend on the ground state electronic structure. Therefore, so to gain a better understanding of these molecular geometries, the main structural parameters of the studied complexes in the S_0 and T_1 states are summarized in Table 1. As shown in Table 1, negligible changes (within<0.005 Å) have also been found on the Pt–N (Pt–N_1 and Pt–N_2) and Pt–C (Pt-C_1 and Pt-C_2) bond lengths at the optimized S_0 geometries of the four complexes, indicating that introducing different substituents into the σ-alkynyl auxiliary of platinum(II) complexes causes minor effect on the geometric structures of these complexes. Additionally, it should be noted that the bond lengths of Pt–N (Pt–N_1 and Pt–N_2) are both significantly longer than those of Pt–C (Pt-C_1 and Pt-C_2), suggesting that the interaction between the phenyl ring and the heavy metal center can be expected to be enhanced to some extent. The hybrid N atom can provide a lone-pair of electrons to form the coordination bond with the Pt center. However, the coordination bond between C and Pt ion is formed just by sharing electrons originating from the two carbon atoms.

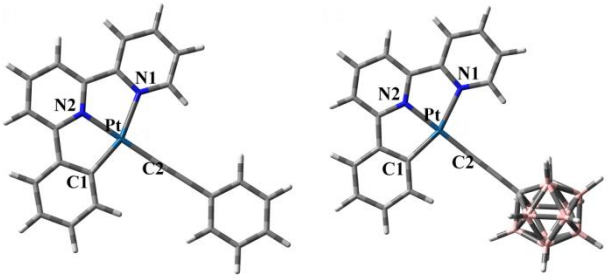

Figure 1 Optimized geometry structures of complex **1** (left) and **4** (right) in the ground state.

Table 1 Main bond lengths (Å), angles (°) and dihedral angles (°) of the complexes **1-4** in the ground state S_0 and the lowest-lying triplet state T_1.

	1		2		3		4	
	S_0	T_1	S_0	T_1	S_0	T_1	S_0	T_1
Pt-N_1	2.156	2.134	2.158	2.131	2.160	2.135	2.159	2.096
Pt-C_1	1.988	2.008	1.987	2.003	1.988	2.007	1.989	1.951
Pt-N_2	2.007	1.980	2.008	1.990	2.010	1.979	2.009	1.991
Pt-C_2	1.956	1.900	1.956	1.917	1.953	1.898	1.951	1.969
C_2-Pt-N_1	101.9	101.6	101.8	101.6	101.9	101.5	102.6	101.2
N_2-Pt-C_1	81.9	81.7	81.9	81.6	81.9	81.8	81.9	82.2
N_1-Pt-N_2	77.9	78.8	77.9	78.7	77.8	78.7	77.8	79.0
C_1-Pt-C_2	98.3	97.9	98.4	98.0	98.3	98.0	97.7	97.5
C_2-C_1-N_2-N_1	-0.030	0.485	-0.339	-0.154	-0.424	0.745	-0.057	-0.276

As shown, by comparing the main bonds in the S_0 and T_1 states for the studied complexes, the bond lengths between Pt metal and other atoms are shortened except that of Pt-C_1. The calculated dihedral angles of C_2-C_1-N_2-N_1 for complex **1-4** are 0.515, 0.493, 1.169 and 0.219, respectively, and obviously, complex **4** has the smallest change among the four complexes. According to the law of energy gap,[49] the greater the structure distortion is, the faster the nonradiation transition becomes. So it can be inferred that the nonradiation decay rate constant of complex **4** may be minimal.

For some transition metal complexes, the intermolecular interactions in solid state or in high concentration solution lead to a triplet-triplet annihilation and concentration quenching and thereby result in lower phosphorescence quantum yield.[28] For exploring the intermolecular interactions further, the two adjacent segments are stacked in the head-to-tail direction.[50] Actually, the intermolecular Pt ··Pt interactions play a key role in the close packing of molecules.[51, 52] The Pt ··Pt distances ($r_{Pt\text{-}Pt}$) of four studied complexes are obtained from the lowest point of potential energy surface as shown in Figure S1. Seen from the Figure S1 and S2, a significantly longer Pt···Pt distance of 5.3 Å is observed in **4** with o-carborane added,compared with that of **1** (3.6 Å), indicating the absence of intermolecular Pt ··Pt interactions between the two paired molecules in complex **4**. Therefore, it can be supposed that the bulkiness of *o*-carborane can effectively prevent formation of close Pt−Pt contacts and thus inhibit triplet−triplet annihilation.

Frontier molecular orbitals

To probe into the electronic absorption and luminescent properties of complexes **1**−**4**, the highest occupied molecular orbital (HOMO) and lowest unoccupied molecular orbital (LUMO) distribution, energy levels, and HOMO−LUMO energy gaps (E_g) are investigated and the obtained results are displayed in Figure 2. Furthermore, more detailed descriptions of molecular orbital, including energies of metal and ligand orbitals, MO compositions and the contribution of different parts are presented in Tables S3–S6.

It is obvious that the electron density of LUMOs of these complexes is rather similar. The LUMOs of the four complexes are nearly distributed on two phenyl rings of the phbpy ligands. However, the relatively significant differences are observed for the HOMOs electron density distribution. The HOMOs mainly reside on π(C≡C-L) (L refers to the substituent groups) and less on d(Pt) in complexes **1-3**, while for complex **4**, the HOMO is mainly contributed by d(Pt) and π(phbpy) (phbpy=6-Phenyl-2,2'-bipyridine) ligands, indicating that the incorporation of *o*-carborane group causes obvious difference in HOMO electron density distribution. Based on the variation of the electron density distribution, four complexes probably have a prominently ligand-centred (LC) charge transfer character. For complex **4,** more d(Pt) orbitals are involved in the HOMO while little in LUMO, which signifies the obvious MLCT nature for the transition HOMO→LUMO, which is favrable to the improvement of electroluminescent efficiency.

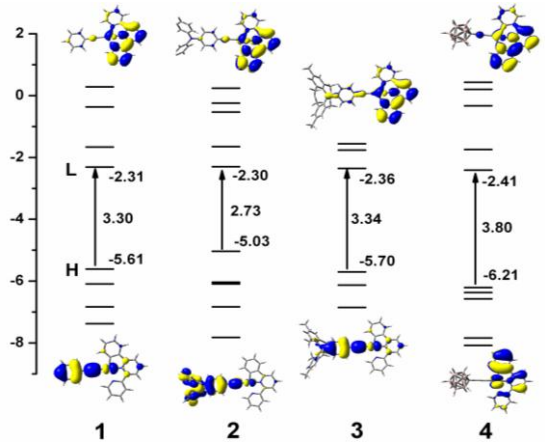

Figure 2 Calculated energy levels, energy gaps, and orbital composition distribution of the HOMO and the LUMO for complexes **1-4** at their S_0 optimized geometries.

It is known that E_g have a great influence on the properties of the complexes. As shown in Figure 2, the introduction of different substituents causes slight effects on the LUMO energy levels but large impacts on the HOMO energy levels of these ligands. With the increase of the electron-withdrawing capabilities of substituents, lower HOMO level and larger E_g can be obtained. The energy gaps of these studied complexes increase as the following: **2** (2.73 eV) < **1** (3.30 eV) < **3** (3.34 eV) < **4** (3.80 eV). Of which complex 4 with *o*-carborane substituted has the maximal E_g, thus a most obvious blue-shifted emission band can be observed. These findings would be useful to the comprehension of the trend of absorption and emission spectra properties further.

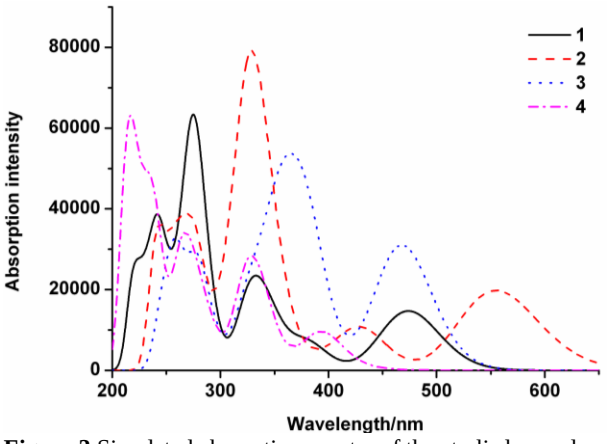

Figure 3 Simulated absorption spectra of the studied complexes at their optimized S_0 geometries in CH_2Cl_2 medium.

Absorption spectra

The TDDFT method has been considered to be a reliable approach in providing satisfactory analysis on the lowest-lying triplet and singlet excited states of heavy metal complexes recently.[53] To compare the electronic transition properties of these complexes in the absorption process, three different functionals (PBE0, B3LYP, and M062X) were performed to study the absorption spectra of **1**. Our results indicate that PBE0 is more accurate for the studied complexes in reproducing the experimental data (Table S2), thereby, the TDDFT/PBE0 method with PCM in CH_2Cl_2 medium is adopted on the basis of the optimized geometries of the ground state. The simulated Gaussian-type absorption curves for the studied complexes are presented in Figure 3 and the excitation energies and transition characters for first singlet and triplet states are listed in Table 2. Furthermore, more detailed analyses of the molecular orbital compositions and the transition informations including absorption energies, dominant configurations, and transition natures of the selected excited states with large oscillator strengths (*f*) are listed in Table S7, along with the experimental data for **1**.

Table 2 Excitation energy, wavelength, oscillator strength (*f*) and transition character for the studied complexes.

	State	λ (nm)/E(eV)	*f*	Configuration[a]	Character
1	S_1	474/2.61	0.1869	H→L (98%)	MLCT/LLCT
	T_1	516/2.40	0.0000	H→L (78%)	MLCT/LLCT
2	S_1	555/2.24	0.2568	H→L (96%)	LLCT
	T_1	530/2.34	0.0000	H→L (78%)	LLCT
3	S_1	468/2.65	0.3963	H→L (97%)	MLCT/LLCT
	T_1	554/2.24	0.0000	H→L (68%)	MLCT/LLCT
4	S_1	437/2.84	0.0048	H→L (95%)	MLCT/LLCT
	T_1	494/2.51	0.0000	H→L (81%)	MLCT/LLCT

[a] H=HOMO, L=LUMO

Combining Table 2 with Figure 3, for all complexes other than **2**, it can be observed that the $S_0 \rightarrow S_1$ and $S_0 \rightarrow T_1$ transitions mainly originate from the HOMO with the significant mixed character of d(Pt)-orbital and phbpy (C≡C-L) based π orbitals to the LUMO with phbpy based π* orbitals, which can be described as mixed MLCT /LLCT characters. However, for **2**, the assignment of $S_0 \rightarrow S_1$ and $S_0 \rightarrow T_1$ excitations are LLCT characters, because the HOMO is consisted of π(C≡C-L) and the LUMO is mainly contributed by π^*(phbpy).

As seen from Table S7, the $S_0 \rightarrow S_1$ absorptions of **1**-**4** are at 474, 555, 468 and 437 nm, respectively, indicating that compared with 1, 2 has an obvious red-shifted absorption band, while 3 and 4 have blue-shifted band, consistent with the trend of the HOMO→LUMO energy gaps. It is concluded that the photophysical and luminescent characteristics of these Pt(II) complexes can be tuned by introducing different substituents into the *σ*-alkynyl auxiliary. Moreover, with the increase of the electronegativity of these substituents, the extent of blue shift becomes greater.

Phosphorescence in dichloromethane medium

To better explore the phosphorescence emissive properties, the 0-0 and $T_1 \rightarrow S_0$ vertical transition energies as well as the values obtained from TDDFT have been computed on the basis of the present DFT results. The 0-0 transition energies ($E_{0\text{-}0}$) are the energy differences in view of zero-point energies (ZPE) between S_0 and T_1 states at their respective optimized geometries. While, according to the ΔSCF method, the vertical transition energies (E_{vert}) are obtained by calculating the electronic-energy differences between the T_1 optimized and S_0 states at the optimized T_1 geometry. The TDDFT results (E_{TD}) are calculated at the optimized T_1 geometry based on the PCM-PBE0 level of theory in CH_2Cl_2 medium. The calculated results, including $E_{0\text{-}0}$, E_{vert} and E_{TD}, are all listed in Table 3, together with the experimental data for complex **1**.

Table 3 The calculated lowest-lying triplet energy values in CH_2Cl_2 for the studied complexes.

	1	2	3	4
$E_{0\text{-}0}$	576	690	563	519
E_{vert}	649	813	637	591
E_{TD}	688	835	679	627
$E_{exp.}$[a]	582			

[a] The experimental value obtains from Reference 19.

As shown in Table 3, compared with the experimental data of complex **1**, the $E_{0\text{-}0}$ provides a better accuracy than both E_{vert} and E_{TD} and the deviation is only 6 nm, much smaller than the two others. Therefore, the $E_{0\text{-}0}$ is reliable for this work to investigate the emissive wavelength.[54, 55] The calculated $E_{0\text{-}0}$ for **1**-**4** follow the order: **2** (690 nm) > **1** (576 nm) > **3** (563 nm) > **4** (519 nm), indicating that there are blue shift of the emission bands for triarylboryl and o-carborane but red shift for triphenylamine. It is indicated that with the enhancing of electronegativity, the degree of blue-shift increases, which is in accordance with the conclusion drawn in the above analysis of FMOs.

Radiative decay rate

The phosphorescent properties for complexes **1**-**4** have been theoretically evaluated through one-component scalar relativistic ZORA TDDFT calculations with spin-orbit coupling (SOC) included, based on the optimized T_1 geometries.[56] The calculated results containing ZFS parameters, radiative rate constants of spin sublevel α(α =1, 2, 3) k_r^{α} and the average radiative decay rate constant k_r and radiative decay lifetimes τ_r of all complexes are collected in Table 4, along with the experimental value of k_r ($k_r=\Phi_{PL}/\tau_{exp}$) for complex **1**. The calculated k_r has the same order of magnitude with the value in experience, which fully demonstrates that the way of computing is feasible.

Table 4 Radiative decay rate constant k_r (s^{-1}), ZFS parameters (cm^{-1}) and radiative decay lifetimes τ_r (μs) for the studied complexes, along with the available experimental values of **1**.

	1	2	3	4
ΔE_{1-2}	8.15	3.95	7.34	17.34
ΔE_{1-3} (ZFS)	26.54	12.26	24.44	32.50
k_r^1	2.44E+04	8.80E+03	5.26E+04	2.71E+05
k_r^2	1.01E+05	3.45E+04	6.83E+04	1.17E+05
k_r^3	8.18E+04	2.28E+04	8.90E+04	4.37E+05
k_r	6.91E+04	2.20E+04	7.00E+04	2.75E+05
τ_r	14.47	45.45	14.29	3.64
$k_{r,exp}$ [a]	10.0E+04			

[a] The experimental value obtains from Reference 19.

As shown in Table 4, the trend of k_r values, equal to the inverse of τ_r, are arranged in the following order: **2** (2.20×10^4 s^{-1}) < **1** (6.91×10^4 s^{-1}) < **3** (7.00×10^4 s^{-1}) < **4** (2.75×10^5 s^{-1}). It means that complex **4** is expected to have higher phosphorescence quantum yield (Φ_{PL}) to some extent owing to the largest k_r of complex **4**. Compared with **1**, **3** and **4** have larger k_r and smaller τ_r. Nevertheless, **2** was just the opposite, which indicates that introducing the substituent with strong electronegativity into the σ-alkynyl auxiliary of tridentate cyclometalated platinum(II) complexes can facilitate radiative decay process and reduce emission decay time. Yersin et al. have reported that it is impossible to characterize the orbital nature of the emiting triplet state, especially the amount of ^{3}MLCT character, based on the ZFS and there is a very interesting trend that the stronger SOC effect is, the larger ZFS values are, thus the greater radiative decay rate constants are.[57-59] However, in Table 4, the ZFS values increase as the following trend: **2** (12.26 cm^{-1}) < **3** (24.44 cm^{-1}) < **1** (26.54 cm^{-1}) < **4** (32.50 cm^{-1}), which are not completely consistent with the trend of k_r values.

In order to further explore radiative decay process in detail, according to eq (3) and (4), the radiative rate constant is governed by three factors, including the transition dipole moments $\mu(S_n)$ for S_0–S_n transitions, singlet–triplet splitting energies $\Delta E(S_n–T_1)$ and the SOC matrix elements $\langle T_1|\ H_{SOC}|\ S_n\rangle$, whose values for the first few excited singlet states of complexes **1-4** calculated by PBE0+SOC-TDDFT+COSMO in CH_2Cl_2 medium at their respective T_1 optimized geometries are presented in Table S7，[60] as well as, the excited singlet states with the higher SOC matrix elements $\langle T_1|\ H_{SOC}|\ S_n\rangle$ are listed in Table 5.

Table 5 Transition dipole moments $\mu(S_n)$ (Debye) for S_0–S_n transitions, singlet–triplet splitting energies $\Delta E(S_n–T_1)$ (eV) and the SOC matrix elements $\langle T_1|\ H_{SOC}|\ S_n\rangle$ (cm^{-1}) of complexes 1-4.

1				2			
S_n	$\mu(S_n)$	$\Delta E(S_n–T_1)$	$\langle T_1\|\ H_{SOC}\|\ S_n\rangle$	S_n	$\mu(S_n)$	$\Delta E(S_n–T_1)$	$\langle T_1\|\ H_{SOC}\|\ S_n\rangle$
S_2	0.81	0.639	445.783	S_2	0.73	0.975	342.644
S_3	0.29	0.648	430.908	S_3	0.30	1.003	317.093
S_4	0.47	1.001	1037.652	S_5	0.44	1.332	792.857
3				4			
S_n	$\mu(S_n)$	$\Delta E(S_n–T_1)$	$\langle T_1\|\ H_{SOC}\|\ S_n\rangle$	S_n	$\mu(S_n)$	$\Delta E(Sn–T_1)$	$\langle T_1\|\ H_{SOC}\|\ S_n\rangle$
S_2	0.74	0.644	406.137	S_2	1.63	0.692	454.186
S_3	0.53	0.661	391.018	S_3	1.46	0.778	548.596
S_4	0.49	1.026	946.558	S_4	0.52	0.880	878.782

[a] The SOC matrix elements $\langle T_1|\ H_{SOC}|\ S_n\rangle$ that are less than or equal to absolute value of 300 $cm^{-1}$are not listed.

The larger $\langle T_1|\ H_{SOC}|\ S_n\rangle$ and $\mu(S_n)$ as well as the smaller $\Delta E(S_n–T_1)$ are supposed to result in higher k_r on the basis of eq 2. Compared with **1**, complex **2** has larger $\Delta E(S_n–T_1)$ and smaller $\mu(S_n)$ and $\langle T_1|\ H_{SOC}|\ S_n\rangle$, leading to a lower k_r, that is, it has quite long phosphorescent lifetimes, which may cause triplet–triplet annihilation in OLEDs. These conclusions are in accordance with the calculated results in Table 4. However, for the coupling S_n (n = 2, 3, 4) state of **1**, **3** and **4**, complex **4** has modest values of $\Delta E(S_n–T_1)$ and $\langle T_1|\ H_{SOC}|\ S_n\rangle$, as well as the obviously stronger $\mu(S_n)$, which indicates that **4** has the highest k_r. Meanwhile, it means that $\mu(S_n)$ is the main factor influencing the radiative decay process. As we know, the ZFS is a reliable parameter to characterize the size of the $T_1 \rightarrow S_n$ SOC effect, that is, the $\langle T_1|\ H_{SOC}|\ S_n\rangle$ value. Compared with **1**, while the $\langle T_1|\ H_{SOC}|\ S_n\rangle$ of **3** is smaller, the $\mu(S_n)$ is greater. It is why complex **3** has smaller ZFS but higher k_r than **1**.

Nonradiative decay rate

According to the energy gap law,[49] the structural distortions parameter β and the energy gap between the T_m and S_0 states are regarded as two major factors governing the nonradiative decay rate constants. On the basis of the analyses of geometries of S_0 and T_1 States above, it can be found that **4** has the smallest structural change, which

indicates that it may possess a smaller nonradiative decay rate. In addition, the energy gaps between T_m and S_0 states for the four complexes are 41.6, 34.2, 42.1 and 45.6 kcal mol^{-1}, respectively, which also indicates that **4** may have the smallest nonradiative decay rate constant k_{nr}. Based on the above analyses, we can conclude that **4** is supposed to have the smallest nonradiative decay rate constant among the four complexes, which is expected to present a higher phosphorescence quantum yield.

Conclusions

The electronic structures and phosphorescent properties of tridentate mononuclear cyclometalated platinum(II) acetylide complexes **1-4** were systematically investigated via the DFT and TDDFT calculations in our work to shed light on the influence of introducing different substituents into the *σ*-alkynyl auxiliary. Among these substituents, the carborane merits have become the focus of our attention. It has been observed that the incorporation of carborane substituent on the *σ*-alkynyl auxiliary ligand effectively stabilizes the HOMO level by a strong inductive electron-withdrawing effect. It should also be noted that with the increase of the electron-withdrawing capabilities of substituents, a lower HOMO level and larger HOMO–LUMO gap can be obtained, which means a blue shift in the emission band. Furthermore, we also investigated the phosphorescence quantum efficiency of the studied complexes through a qualitative analysis of k_{nr} by the energy gap law and calculations on k_r including $\mu(S_n)$ for S_0–S_n transitions, $\Delta E(S_n–T_1)$ and the SOC matrix elements $\langle T_1| H_{SOC}| S_n \rangle$ by the TDDFT approach. Thereinto, complex **4** has the largest k_r and the smallest k_{nr}. The bulkiness of *o*-carborane hinders the intermolecular interactions and thereby restrains triplet−triplet annihilation. The foregoing calculated results suggest that the incorporation of *o*-carborane can give rise to a significant blue shift of the phosphorescence band and a greater phosphorescence quantum yield. Hence, we hope this work can provide a helpful guidance for the further design of highly efficient emitters applied in OLEDs..

Notes and references

1. D. Escudero, E. Heuser, R. J. Meier, M. Schäferling, W. Thiel and E. Holder, *Chemistry-A European Journal*, 2013, **19**, 15639-15644.
2. J. Han, X. Chen, L. Shen, Y. Chen, W. Fang and H. Wang, *Chemistry-A European Journal*, 2011, **17**, 13971-13977.
3. R. Liu, J. Chang, Q. Xiao, Y. Li, H. Chen and H. Zhu, *Dyes and Pigments*, 2011, **88**, 88-94.
4. Y. Liu, X. Sun, Y. Wang and Z. Wu, *Dalton Transactions*, 2014, **43**, 11915-11924.
5. M. A. Baldo, S. Lamansky, P. E. Burrows, M. E. Thompson and S. R. Forrest, *Applied Physics Letters*, 1999, **75**, 4 - 6.
6. P. Shao, Y. Li, A. Azenkeng, M. R. Hoffmann and W. Sun, *Inorganic chemistry*, 2009, **48**, 2407-2419.
7. M. Tanaka and H. Mori, *The Journal of Physical Chemistry C*, 2014, **118**, 12443-12449.
8. S. Zhang, Y. Si and Z. Wu, *RSC Advances*, 2014, **4**, 15849-15855.
9. A. Chakraborty, J. C. Deaton, A. Haefele and F. N. Castellano, *Organometallics*, 2013, **32**, 3819-3829.
10. X. Zhou, Q.-J. Pan, B.-H. Xia, M.-X. Li, H.-X. Zhang and A.-C. Tung, *The Journal of Physical Chemistry A*, 2007, **111**, 5465-5472.
11. T. WA, F. GR, M. L, B. AM, K. R and W. JA., *Inorganic Chemistry*, 2014.
12. C. Yu, K. M. C. Wong, K. H. Y. Chan and V. W. W. Yam, *Angewandte Chemie*, 2005, **117**, 801-804.
13. L. Y, T. DP, C. CK, W. KM, C. MY and Y. VW., *Chemistry - A European Journal*, 2014, **20**, 13710–13715.
14. Q.-Z. Yang, L.-Z. Wu, Z.-X. Wu, L.-P. Zhang and C.-H. Tung, *Inorganic chemistry*, 2002, **41**, 5653-5655.
15. V. DA, L. Q, C. YH and H. S, *Journal of inorganic biochemistry*, 2014, **134**, 49–56.
16. D. Zhang, L.-Z. Wu, L. Zhou, X. Han, Q.-Z. Yang, L.-P. Zhang and C.-H. Tung, *Journal of the American Chemical Society*, 2004, **126**, 3440-3441.
17. R. Liu, Y. Li, Y. Li, H. Zhu and W. Sun, *The Journal of Physical Chemistry A*, 2010, **114**, 12639-12645.
18. C. Latouche, P.-H. Lanoë, J. A. G. Williams, V. Guerchais, A. Boucekkine and J.-L. Fillaut, *New J. Chem.*, 2011, **10**, 2196-2202.
19. L. W, M. BX, C. MC, H. Z, C. CM, Z. N and L. ST., *J Am Chem Soc*, 2004, 4958-4971.
20. W. Wu, D. Huang, X. Yi and J. Zhao, *Dyes and Pigments*, 2013, **96**, 220–231.
21. J. F. Valliant, K. J. Guenther, A. S. King, P. Morel, P. Schaffer, O. O. Sogbein and K. A. Stephenson, *Coordination Chemistry Reviews*, 2002, **232**, 173–230.
22. L. Zhang, L. Tian, M. Li, R. He and W. Shen, *Dalton Trans.*, 2014, **17**, 6500-6512.
23. X. Yang, X. Xu, J. Zhao, J.-s. Dang, Z. Huang, X. Yan, G. Zhou and D. Wang, *Inorganic chemistry*, 2014.
24. L. Y, S. X, W. Y and W. Z., *Dalton Trans.*, 2014, **31**, 11915-11924.
25. B. BA, K. SB, L. JS, S. LF and W. S., *Dalton Trans*, 2013, **28**, 10089-10092.
26. A. M. Prokhorov, T. Hofbeck, R. Czerwieniec, A. F. Suleymanova, D. N. Kozhevnikov and H. Yersin, *J.am.chem.soc*, 2014, **136**.

27. P. AM, S. PA, R. VL, K. VN and K. DN, *Chem： commun*, 2011, **47**, 7713-7715.
28. C. Shi, H. Sun, Q. Jiang, Q. Zhao, J. Wang, W. Huang and H. Yan, *Chemical Communications*, 2013, **49**, 4746-4748.
29. T. Kim, H. Kim, K. M. Lee, Y. S. Lee and M. H. Lee, *Inorg. Chem.*, 2012, **52**, 160-168.
30. K. T, K. H, L. KM, L. YS and L. MH., *Inorg. Chem.*, 2012, **52**, 160-168.
31. A. D. Becke, *The Journal of Chemical Physics*, 1993, **98**, 1372-1377.
32. J. P. Perdew, J. A. Chevary, S. H. Vosko, K. A. Jackson, M. R. Pederson, D. J. Singh and C. Fiolhais, *Physical Review B*, 1992, **46**, 6671-6687.
33. Z. Y and T. DG, *Acc. Chem. Res.*, 2008, **41**, 157-167.
34. W. R. Wadt and P. J. Hay, *Journal of Chemical Physics*, 1985, **82**, 284-298.
35. L. C, Y. W and P. RG., *Physical review. B, Condensed matter*, 1988, **37**, 785-789.
36. M. S. Gordon, *Chemical Physics Letters*, 1980, **76**, 163–168.
37. T. Helgaker and P. Jo/rgensen, *Journal of Chemical Physics*, 1991, **95**, 2595-2601.
38. J. Autschbach, T. Ziegler, S. J. A. v. Gisbergen and E. J. Baerends, *Journal of Chemical Physics*, 2002, **116**, 6930-6940.
39. A. D. Becke, *Physical Review. A*, 1988, **38**, 3098-3100.
40. C. C. Chambers, G. D. Hawkins, C. J. Cramer and D. G. Truhlar, *J. Phys. Chem.*, 1996, **100**, 100--16385.
41. P. J. Hay and W. R. Wadt, *Ab initio effective core potentials for molecular calculations. Potentials for K to Au including the outermost core orbitals - ResearchGate*, 1985, **82**, 299-310.
42. Frisch M J, Trucks G W, Schlegel H B, et al. J, Fox, DJ (2009) Gaussian 09, Revision A. 01.. Gaussian[J]. Inc., Wallingford, CT.
43. H. Yersin, A. F. Rausch, R. Czerwieniec, T. Hofbeck and T. Fischer, *Coordination Chemistry Reviews*, 2011, **255**, 2622-2652.
44. G. t. Velde, F. M. Bickelhaupt, E. J. Baerends, C. F. Guerra, S. J. A. v. Gisbergen, J. G. Snijders and T. Ziegler, *Journal of Computational Chemistry*, 2001, **22**, 2001.
45. C. Fonseca Guerra , J. G. Snijders , G. te Velde and E. J. Baerends, *Theoretical Chemistry Accounts*, 1998, **99**, 391-403.
46. E. v. Lenthe, J. G. Snijders and E. J. Baerends, *The Journal of Chemical Physics*, 1996, **105**, 6505-6516.
47. A. Klamt and G. Schüürmann, *Journal of the Chemical Society, Perkin Transactions 2*, 1993, **5**, 799-805.
48. E. A. Jonas, R. J. Knox, L. K. Kaczmarek, J. H. Schwartz, D. H. Solomon, E. A. Jonas, L. K. Kaczmarek, J. H. Schwartz and D. H. Solomon, *The Journal of Neuroscience*, 1996, 1645-1658.
49. J. S. Wilson, N. Chawdhury, M. R. A. Al-Mandhary, M. Younus, M. S. Khan, P. R. Raithby, A. Köhler and R. H. Friend, *Journal of the American Chemical Society*, 2001.
50. S. Huo, C. F. Harris, D. A. Vezzu, J. P. Gagnier, M. E. Smith, R. D. Pike and Y. Li, *Polyhedron*, 2013, **52**, 1030-1040.
51. Y. Chen, *Angewandte Chemie*, 2009, **48**.
52. X. Yang, X. Xu, J. Zhao, J. S. Dang, Z. Huang, X. Yan, G. Zhou and D. Wang, *Inorganic Chemistry*, 2014, **53**.
53. Y. L. Li, L. Han, Y. Mei and J. Z. H. Zhang, *Chemical Physics Letters*, 2009, **482**, 217–222.
54. X. Li, B. Minaev, H. Ågren and H. Tian, *European Journal of Inorganic Chemistry*, 2011, **2011**, 2517–2524.
55. Z. L, T. L, L. M, H. R and S. W, *Dalton Trans.*, 2014, **43**, 6500-6512.
56. Y. Wu, S.-X. Wu, H.-B. Li, Y. Geng and Z.-M. Su, *Dalton Transactions*, 2011, **40**, 4480-4488.
57. W. J. Finkenzeller, T. Hofbeck, M. E. Thompson and H. Yersin, *Inorg. Chem.*, 2007, **46**, 5076-5083.
58. H. Yersin, A. F. Rausch and R. Czerwieniec, *Physics of Organic Semiconductors, Second Edition*, 2013.
59. H. Yersin and H. Yersin, *Triplet Emitters for OLED Applications. Mechanisms of Exciton Trapping and Control of Emission Properties*, Transition Metal and Rare Earth Compounds, 2004.
60. Y. Wu, G.-G. Shan, H.-B. Li, S.-X. Wu, X.-Y. Ren, Y. Geng and Z.-M. Su, *Physical Chemistry Chemical Physics*, 2015, **17**, 2438-2446.

Graphical abstract:

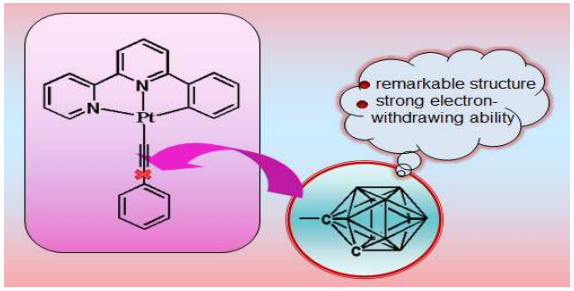

Introducing *o*-carborane leads to significant blue-shifted emission band and obviously-higher electroluminescent efficiency via systemic and in-depth theoretical studies.